JOURNAL OF MATERIALS SCIENCE 10 (1975) 705–713

Oxidation stacking faults in epitaxial silicon crystals

M. CONTI, G. CORDA, R. MATTEUCCI
SGS-ATES Componenti Elettronici, Milano, Italy

C. GHEZZI
Laboratorio MASPEC del C.N.R., Parma, Italy

Oxidation stacking faults (SFs) in epitaxial silicon crystals have been studied by means of preferential etch and X-ray topography. SFs lie on {111} planes and are surrounded by a partial Frank dislocation. Nucleation takes place at crystallographic defects located near the surface of epitaxial layers. These defects appear as etch hillocks after preferential etch. SF length as a function of temperature and time for different thermal treatments is reported. The SF length is controlled by an activation energy of 2.6 eV. This energy, which is nearly half the self diffusion activation energy of silicon, supports a SF growth mechanism controlled by vacancy emission.

1. Introduction

Stacking faults (SFs) are known to nucleate at the silicon crystal surfaces during thermal oxidation [1-13]. Their presence influences the performance of silicon devices processed therein. Electrical effects of SFs are soft reverse characteristics in p–n diodes [2], short circuits between collector and emitter junctions in bipolar transistors known as "pipes" [11] and a strong low frequency or eventually burst-type excess noise in transistors and ICs [14].

For a SF to be nucleated there must be a defect present at the silicon surface. This can be introduced by mechanical polishing with SiC paper [1-3], by HF acid attack [4], by heat-treatment, or by surface contamination. Wilheim and Joshi [5] observed the nucleation of oxidation SFs in silicon wafers without any mechanical damage, and Ravi and Varker reported SF nucleation at the oxygen-vacancy complexes present in swirl-affected wafers [6].

The present work deals with oxidation SFs which are relatively frequent in epitaxial silicon layers and nucleate at surface defects typical of the epitaxial process. The dependence of SF length on oxidation time, temperature and atmosphere is presented.

Contrast analysis of X-ray topographs confirms the extrinsic nature of these SFs. Depth-to-length ratio, the influence of semiconductor type, resistivity and oxygen content are presented and discussed.

2. Experimental procedure

Single crystal silicon wafers of (100) and (111) orientation, P-type 2 to 4 Ω cm, grown by Czochralsky technique (CZ) were polished by a chemical-mechanical process and epitaxially grown in a horizontal epi reactor. The epi layer was typically 10 to 12 μm thick, N-type 1 to 2 Ω cm. The epi deposition process was done at 1175°C (optical) and, before heating, the reactor was flushed with nitrogen (4 min) and hydrogen (4 min). Additional experiments were done on epi layers of the same resistivity and thickness grown on float-zone substrate (FZ) and on thicker epi layers (30 μm). Thermal oxidation was performed in open tube furnaces, both in dry and in wet oxygen atmosphere (oxygen bubbling through deionized water at 97°C). The temperature range was 1000 to 1250°C. The silicon dioxide thickness was measured by a Taylor Hobson Talysurf. Crystallographic defects were revealed by preferential etch [15] and by X-ray topography, performed with a modified Picker Lang camera. Cu$K\alpha_1$ and in some cases Mo$K\alpha_1$ radiation was used for recording the topographs on Ilford L4 50 μm nuclear plates. The microanalysis, both dispersive and non-dispersive, was done on the

© *1975 Chapman and Hall Ltd.*

JEOL Scanning electron microscope JSM-50A at CSELT. Oxygen and carbon content was also evaluated by infra-red absorption through a Perkin-Elmer spectrophotometer.

3. Experimental results

3.1. Nucleation and growth of stacking-faults

When a few-second preferential etch is done over an epi wafer, some small etch hillocks can be observed as shown in the microphotograph of Fig. 1 (Nomarsky interference contrast). Their density varies from wafer to wafer and from point to point of the same wafer. Density range is 10^3 to 10^6 cm^{-2}. The hillocks are probably related with some defects present in the epi layer. Epi grown stacking-faults are normally absent (less than 100 cm^{-2}). Oxidation at 1100°C causes the defects to produce a SF. Figs. 2 and 3 show SFs nucleated after 20 and 40 min respectively. Their length increases with oxidation time, temperature and depends on oxidation atmosphere.

Points to be noted are: (i) not all the etch hillocks generate a SF, (ii) the length of SF produced on all the wafers on an oxidation run exhibits a high degree of uniformity.

Dispersive and non-dispersive analysis of electron excited X-ray fluorescence was performed on these hillocks and the related SF. No contaminants of any kind were detected, at least within the sensitivity limits of the instruments. However, the presence of carbon was revealed in some etch hillocks and SFs. Oxygen and carbon content of the epi layer was also investigated on 100 μm layers by a standard infra-red method. To obtain a sufficient sensitivity the substrate was etched away; the remaining epi layer was cut into small rectangular pieces. The pieces were stuck together using opaque wax and the resulting solid was carefully polished in order to obtain good infra-red light transmission parallel to the platelets. Oxygen and carbon contents were found negligible within the sensitivity limit of the method (less than 10^{17} cm^{-3} in the case of oxygen). Most of the SFs generated during thermal oxidation have a uniform length, although there is also a small number of noticeably shorter SFs.

The SF length as a function of reciprocal oxidation temperature is shown in Fig. 4. Oxidation time is constant. When temperatures in the range 1000 to 1150°C are used, the SF length is always controlled by an activation energy of 2.6 ± 0.1 eV independent of whether the substrate orientation is (111) or (100) and the oxidizing atmosphere is dry or wet. At higher temperatures the faults are shorter than predicted by a single activation energy. Wet oxidation produces a 1.8 times longer SF than dry oxidation. Surface orientation is also important since (100) orientation produces faults approxi-

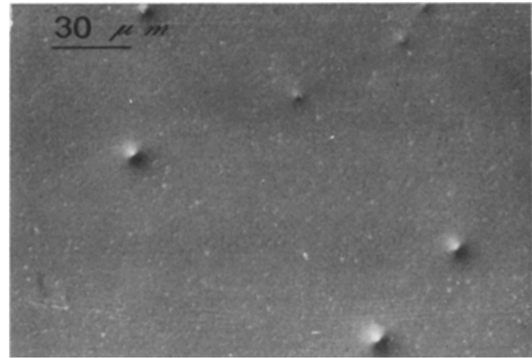

Figure 1 Etch hillocks on epi layer. 30 sec preferential etch.

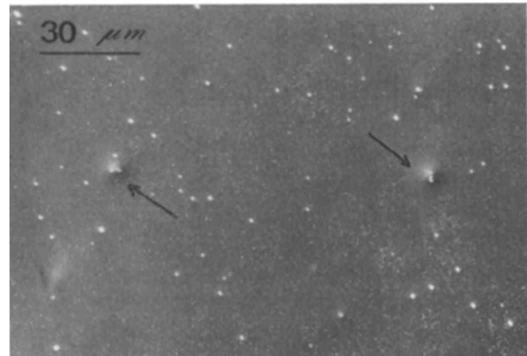

Figure 2 Nucleating SFs at hillocks after 20 min. Dry oxidation at 1100°C, 30 sec preferential etch.

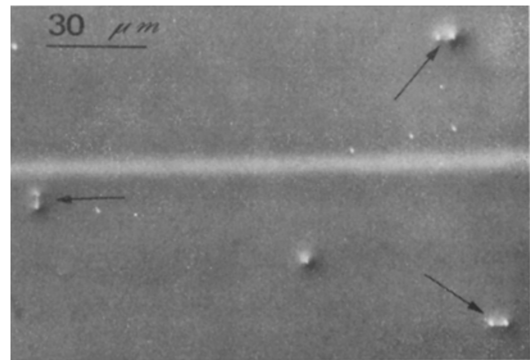

Figure 3 SFs after 40 min. Dry oxidation at 1100°C, 30 sec preferential etch.

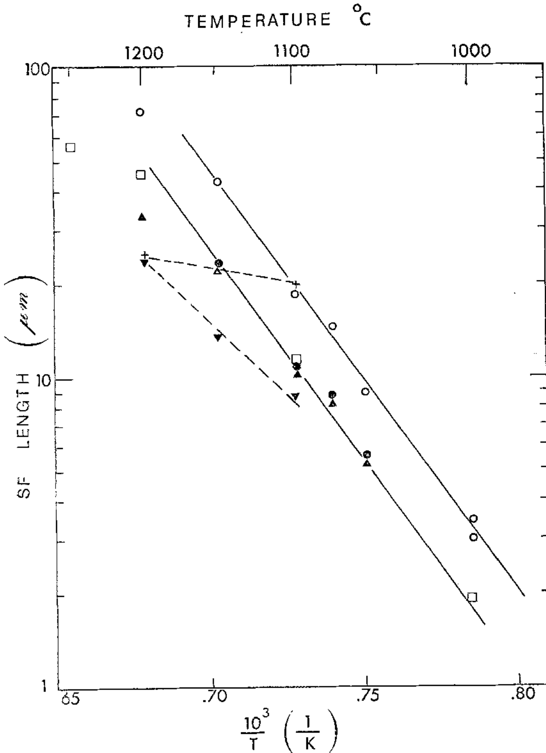

Figure 4 SF length as a function of oxidation temperature for various processes (same processing time).

Key:

Symbol	Reference	Orientation	Oxidation time (min)	Oxidation atmosphere
○	This work	(100)	120	wet O_2
□	This work	(100)	60	wet O_2
▲	This work	(100)	120	dry O_2
●	This work	(111)	510	dry O_2
+	[11]	(100)	20	steam O_2
▼	[11]	(100)	60	wet O_2

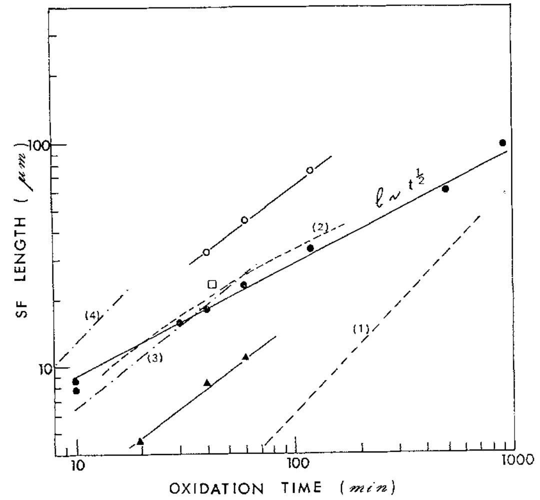

Figure 5 SF length as a function of oxidation time for isothermal processes.

Key:

Symbol	Reference	Orientation	Oxidation temperature (°C)	Oxidation atmosphere
●	This work	(100)	1200	dry O_2
▲	This work	(100)	1100	wet O_2
○	This work	(100)	1200	wet O_2
(1)	[9]	(100)	1100	dry O_2
(2)	[9]	(100)	1100	steam O_2
(3)	[11]	(100)	1200	wet O_2
(4)	[11]	(100)	1200	steam O_2
□	[10]	(100)	1200	wet O_2

mately twice as long as those produced in (111) material. Experimental results obtained by Queisser and Van Loon [11] are also reported in Fig. 4 for comparison (dashed lines). As far as we are concerned with the activation energy, our data are higher than those given by Queisser, however, it has to be noted that these latter data refer to an elevated and small temperature range. In this range, our results should also suggest a lower activation energy.

Fig. 5 shows the SF length as a function of the oxidation time. For sake of completeness, results reported by other authors are also shown (dashed lines). Dry oxidation at 1200°C produces SFs whose length is proportional to the square root of oxidation time. Oxide thickness was measured and was found proportional to the square root of oxidation time, therefore a conclusion is drawn that the SF length is proportional to oxide thickness.

When the steam oxidation process is used, fault length increases even more rapidly with oxidation time. The large discrepancies among the available data in the literature (see Fig. 5) seem to indicate that there are some parameters affecting the SF length which are not always under control. For this reason, we investigated whether the SF length was influenced by some features of the epi layer.

Epi thickness does not seem to have any influence on epi SF length. 30 μm thick epi layers of standard resistivity developed SFs of the same length as the 10 to 12 μm layer even in the case of a SF deeper than 12 μm.

To test the importance of the epi layer, substrates of standard resistivity were processed

TABLE I SF length (μm) for 120 min wet O_2 oxidation on different wafers (see text)

T (°C)	Wafer		
	A	B	C
1060	9	9	9
1080	11	11	12
1120	28	26	25
1175	55	54	56

in the epi reactor without the $SiCl_4$ flush (wafer A). They were subsequently oxidized together with standard substrates (wafer B) and substrates with standard epi layer (wafer C). The results are reported in Table I. The resulting SF length was nearly the same for all three tests. However, the SF density was very low in test B. Finally, dry O_2 oxidation at 1200°C for 915 min on epi layers grown on FZ substrates with less than 10^{17} O_2 cm^{-3} caused the development of SF of the same length (96 μm) as the epi layer grown on standard CZ substrates with 10^{18} O_2 cm^{-3}.

3.2. Morphology and X-ray contrast of stacking-faults

To determine the depth of the SFs, some (100) oxidated epi wafers were alternatively etched with preferential and non-preferential etches. The silicon removed was carefully measured with the Talysurf apparatus.

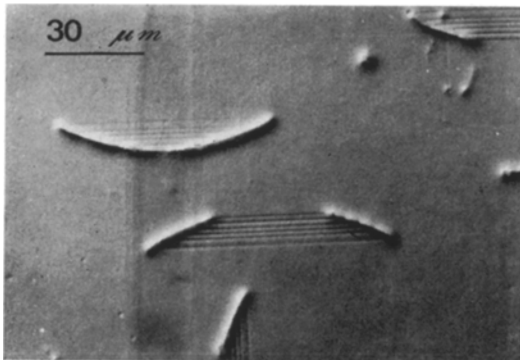

Figure 6 Etch pattern of SFs alternately etched with preferential and non-preferential etch.

Fig. 6 shows a typical etch pattern obtained in these experiments. The elliptical line is the etch pattern of the dislocation line surrounding the SF. The thin straight lines parallel to the SF are due to the subsequent preferential etches. By measuring the distances between such lines and the silicon steps, the plane where the SF lies can be reconstructed. This plane is of the {111} family. The depth of the stacked region can now be easily determined and is found to be approximately $\frac{1}{4}$ of the SF length. Some small differences in the shape of the stacked area and, consequently, of the depth-to-length ratio were found when different times or oxidizing atmospheres were used. The determination of the depth-to-length ratio of SFs in (111) wafers is less accurate, because of their smaller length and because {111} planes lie at a steeper angle to the surface. However, the ratio seems to be essentially the same.

Figure 7 Symmetrical {220} Laue topograph of an oxidized epitaxial silicon wafer. Cu$K\alpha_1$ radiation.

The X-ray images of SFs in (001) oxidized epitaxial silicon wafers were revealed by means of Lang topography. A typical defect pattern for an oxidized sample is shown in Fig. 7. An array of small defects, whose density is strongly inhomogeneous can be seen. These defects were identified as SFs by comparing X-ray images with those observed by optical microscopy after preferential etching. Typical enlarged X-ray

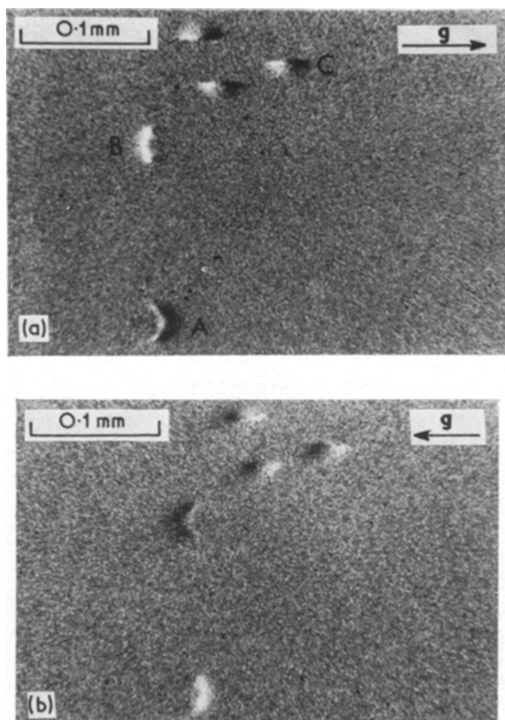

Figure 8 ($\bar{2}20$) (a) and ($2\bar{2}0$) (b) topographs of the same array of defects. Note the inversion of the black-white contrast. Cu$K\alpha_1$ radiation was employed. Images indicated as A, B and C correspond to SFs lying on the ($\bar{1}11$), ($1\bar{1}1$) and (111) or ($\bar{1}\bar{1}1$) planes, respectively.

images of SFs are shown in Fig. 8. This topograph was taken with Cu$K\alpha_1$ radiation ($\mu t = 4.6$) by keeping the back of the wafer turned towards the X-ray source so that the SF pattern was nearest the exit surface of the X-ray beam. In this case the observed contrast was essentially "Friedel contrast" [16] due to tie-point migration on the dispersion surface [17, 18]. This statement was verified by observing inversion of the black-white contrast in (hkl) and ($\bar{h}\bar{k}\bar{l}$) reflections, as shown by comparing Fig. 8a and b. In the present case, the black-white contrast of a defect cannot be explained as being due to its direct and dynamic images, respectively. In fact, since the SF pattern appears at the exit surface of the X-ray beam, the direct and the dynamic images belonging to the same SF should completely overlap. Moreover, the black-white contrast is not visible when the SF pattern is nearest to the surface of entrance of the X-ray beam: this contradicts the hypothesis that the black contrast is due to the direct image of the defect. Finally, with the same hypothesis, one cannot explain why the black image is strongly modified when changing (hkl) into ($\bar{h}\bar{k}\bar{l}$) reflections (see, for example, the images indicated with letters A and B in Fig. 8a and b). This latter feature is discussed below.

Direct images of the defects can be obtained using Mo$K\alpha_1$ radiation ($\mu t = 0.50$). In this case the contrast due to the dislocation loops bounding the faults should be observed, as well as the fringe pattern typical of the SF. In the present case, however, the size of the faults is either smaller than the separation between fringes observed on large SFs [19] or comparable with the calculated "pendellosung" period (6.6 μm for {220} symmetrical reflections in silicon), so that the fringe pattern cannot be observed. It is then likely that the observed contrast is due mainly to the dislocation loops surrounding the faults. The loops, however, cannot be resolved by X-ray methods, since their size is comparable with the width of dislocation images in X-ray topography, therefore the final result is the appearance of diffuse black spots. A comparison between Friedel and direct images for the same array of defects is given in Fig. 9. The direct contrast of the SFs is similar to that observed [20, 21] for SFs formed during thermal oxidation at "swirl"-type defect distributions related to clusters of vacancies and oxygen atoms in the crystal [6].

The direct image can be used to obtain information on the Burgers vector of the dislocation loop surrounding the SF. The analysis of the direct images can be performed as described by Matsui and Kawamura [20]. It was established that the loops are of the Frank type, i.e. their Burgers vectors lie in the $\langle 111 \rangle$ directions. For instance, on ($\bar{2}20$) topographs (see Fig. 9b and d), loops on (111) or ($\bar{1}\bar{1}1$) planes give a systematically faint contrast, in agreement with the fact that the Burgers vectors lie on the reflecting planes. If, on the contrary, the loops were of the Shockley type, statistically, only one third of them should give a faint contrast, because in this case the Burgers vectors may be parallel to the three $\langle 112 \rangle$ directions lying on the fault plane and only one is, therefore, parallel to the reflecting planes. The faint contrast of the loops is due to the pure edge nature of the Frank partial dislocation. The conditions for invisibility of the direct image of a pure edge dislocation line are $\mathbf{g}.\boldsymbol{b} = 0$ and $\mathbf{g} \times \mathbf{n} = 0$, $\mathbf{g}$, $\boldsymbol{b}$ and $\mathbf{n}$ being respectively the diffraction

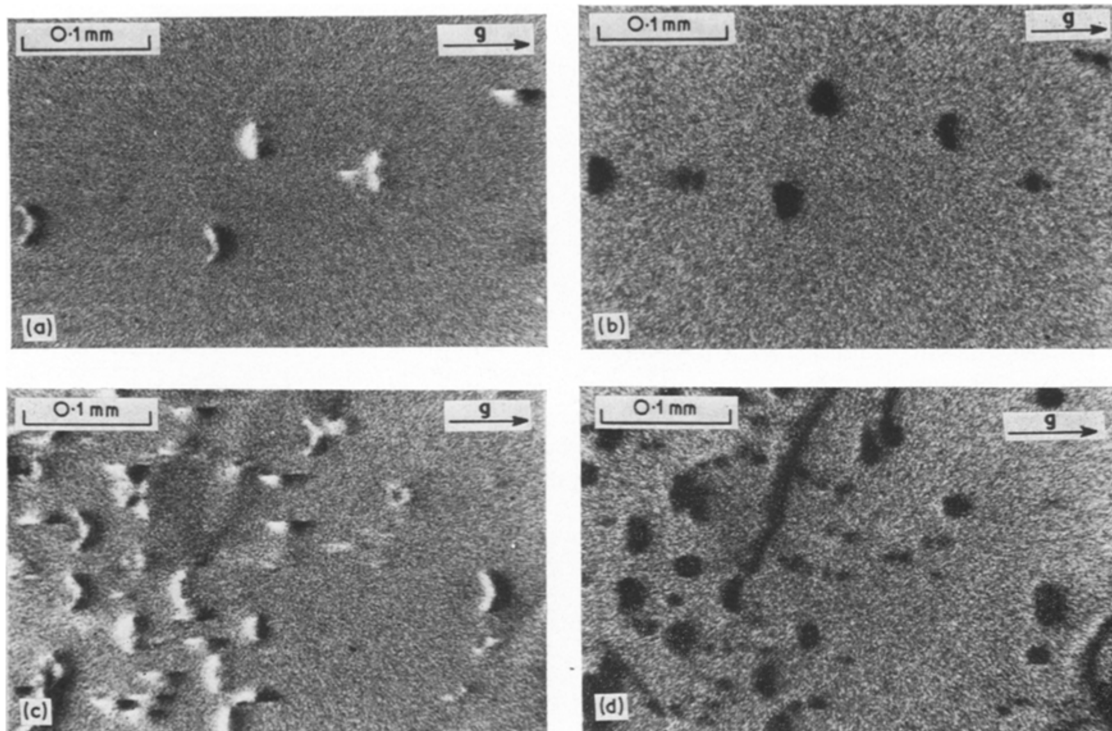

Figure 9 A comparison between Friedel (a and c, Cu$K\alpha_1$ radiation) and direct images (b and d, Mo$K\alpha_1$ radiation).

vector, the Burgers vector and the unit vector along the positive direction of the dislocation line. Frank loops lying on $(\bar{1}\,1\,1)$ or $(1\,\bar{1}\,1)$ planes should give a strong contrast in the $(\bar{2}20)$ topographs since $\mathbf{g}.\boldsymbol{b} \neq 0$. For Frank loops lying on the $(1\,1\,1)$ or $(\bar{1}\,\bar{1}\,1)$ planes the first condition is always satisfied, whereas the second is satisfied only for that part of the loop having $\mathbf{n}$ parallel to the surface of the crystal. Since $\mathbf{g} \times \mathbf{n} \neq 0$ mainly near the two intersections of the loop with the surface, the direct image will be composed of two black spots aligned along the direction of the diffraction vector and separated by a region free of contrast. This is essentially what we could observe through a close inspection of the topograph, a few examples of similar images being shown in Fig. 10.

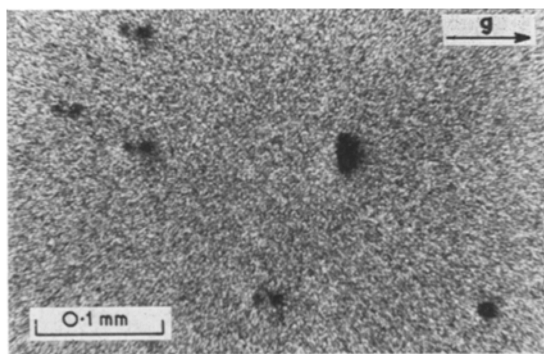

Figure 10 $(\bar{2}20)$ topograph. Mo$K\alpha_1$ radiation. The direct images of dislocation loops bounding faults that lie on the $(1\,1\,1)$ or $(\bar{1}\,\bar{1}\,1)$ planes are composed of two black spots lined up along the direction of the diffraction vector, as expected (see text).

As far as the direct images of the loops surrounding the faults are concerned, we cannot decide if the SFs are of the intrinsic or extrinsic type. This latter information may be obtained from an analysis of the black-white contrast of Friedel images with respect to the sense of the diffraction vector. This analysis allows the determination of the sign of the non-compensated curvature of reflecting planes, the lack of compensation being due to the presence of the crystal surface. In the present case, it was concluded that the SFs are of the extrinsic type for the following reasons.

In Fig. 11, the curvature of the lattice planes

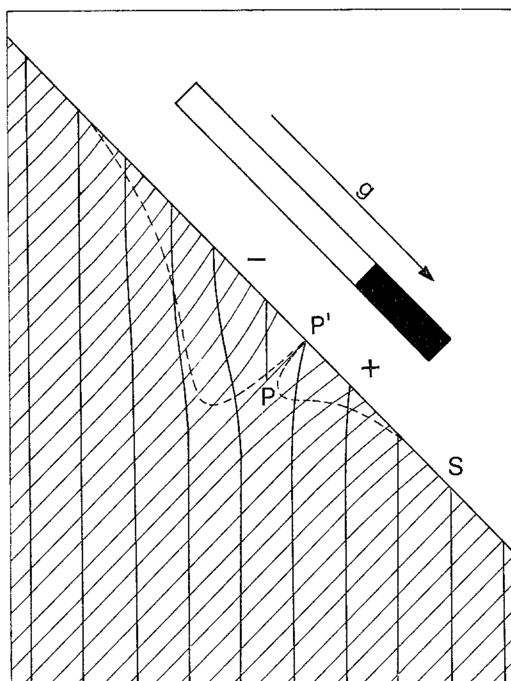

Figure 11 Qualitative sketch of the curvature of the reflecting planes near an extrinsic fault at the exit surface S of the X-ray beam. The drawing, which refers in this case, to the ($\bar{2}20$) reflection, shows a section parallel to the diffraction plane. The expected ordering of the black-white contrast, with respect to the sense of the diffraction vector, is roughly sketched (see text).

near an extrinsic fault is roughly sketched. The drawing shows a section of the crystal parallel to the diffraction plane and refers, for instance, to the ($\bar{2}20$) reflection. The closest spaced planes, which are far from the SF and cut the surface perpendicularly, are the ($\bar{1}10$) reflecting planes, whereas the largest spaced ones are the ($1\bar{1}1$) lattice planes containing an extrinsic fault near the surface. The Frank loop surrounding the fault intersects the plane of the paper at P and its Friedel image should be similar to that indicated by B in Fig. 8a. The dashed lines give, in a qualitative way, the amount of the non-compensated curvature of the reflecting planes as a function of the distance along the surface from the projection P′ of the point P. Three arguments are important: (i) the non-compensated curvature changes sign at P′, so that PP′ gives the trace of the contrast-free plane: this explains the origin of the black-white contrast; (ii) following the argument given in [16], a negative sign for the non-compensated curvature corresponds to a decrease in the scattered intensity, i.e. to a white contrast, and vice versa. The ordering of the black-white contrast with respect to the sense of the diffraction vector is identical to that observed at B in Fig. 8a. Following a similar argument, it is easy to predict the observed contrast at A (Fig. 8a) corresponding to an extrinsic fault lying on the ($\bar{1}11$) planes. The observed Friedel contrast is thus similar to that expected in the case of extrinsic faults; (iii) there is an asymmetry in the extensions of those regions having curvatures of different sign; this explains the asymmetry in the observed black-white contrast.

As a final remark, all the X-ray observations are seen to be consistent with the statement that SFs are of the extrinsic type and are surrounded by Frank partial dislocation loops. A similar result has been frequently reported in the literature for oxidation SFs in silicon and was first given by Booker and Tunstall [22] through contrast analysis of TEM images.

4. Discussion

Crystallographic defects in silicon epi layers, revealed as hillocks after preferential etch, have been shown to be nucleation sites for oxidation SFs. Although it is not known whether they contain carbon precipitates, it seems very likely that a local stress is produced which is the primary cause of SF generation. Another important result is that a thermally-growing oxide layer, whether in a dry or steam atmosphere, is a necessary condition for SF generation.

A nucleation mechanism recently proposed by Ravi and Varker [6] for oxidation SFs assumes an enhanced oxygen diffusion associated with oxygen-vacancy complexes present in swirl-affected silicon wafers.

Oxidation of silicon takes place by the transport of oxygen atoms at the oxide-silicon interface and oxygen continues to diffuse into the silicon lattice up to the solid solubility limit. If the solid solubility limit of oxygen in silicon at the oxidation temperature is exceeded, the oxygen will precipitate. The precipitation takes the form of Frank discs on close-packed planes and a subsequent growth of the discs by vacancy emission is thought to give rise to the observed faults.

For the same mechanism to be effective with epi material, an enhanced oxygen diffusion and concentration in hillock-type defects would be necessary. However, no evidence of such a fact

has been reported. A different model, involving the collapse of interstitial discs of silicon atoms was, therefore, considered. The starting point is the vacancy undersaturation, produced in the silicon lattice near the oxide-silicon interface as a result of the presence of a growing oxide layer. The vacancy undersaturation was experimentally demonstrated by Sanders and Dobson [3] and it is believed to be due to the fact that the diffusing oxygen atoms occupy vacant lattice sites. At a given distance from the interface, the vacancy undersaturation is constant in the absence of crystallographic defects; however, greater undersaturation can be expected at a number of sites where tensile stress predominates: this might be the case for the observed etch hillocks, especially in the case of coherent precipitates of SiC compounds. A first hypothesis is that precipitation of interstitial silicon atoms in the form of extrinsic {111} discs takes place at these sites during cooling following the thermal oxidation process. This hypothesis must, however, be rejected owing to the observed dependence of the SF length on the oxidation time, showing that nucleation and growth of SFs take place during the heat-treatment itself.

The growth of extrinsic faults in the presence of vacancy undersaturation was considered by Prussin [23] who showed that the critical vacancy undersaturation needed to form an extrinsic Frank loop is lowered in the presence of tensile stress. From Prussin's results, one may expect that at elevated temperatures, aggregations of interstitial atoms are continuously formed in the crystal. Such aggregates would most likely consist of a double layer of atoms lying between {111} planes and should be stable, owing to the considerable reduction in the number of dangling bonds. When the layer reaches its critical radius it will collapse to form an extrinsic Frank dislocation loop surrounding a SF. The fault may grow further by vacancy emission processes if the chemical potential of a vacancy is positive and sufficiently high in order that the increase in the elastic energy of the dislocation loop is balanced by a decrease in the free energy due to the vacancy emission process. The chemical potential of a vacancy is given by [23]

$$\mu_v = K_B T \ln \frac{C_0}{C} + P \frac{\partial V(0)}{\partial n}$$

where C_0 and C are, respectively, the equilibrium and actual vacancy concentrations, P is the purely tensile component of the local stress, $V(0)$ is the vacancy formation volume at zero pressure and the derivative is taken with respect to the number of vacancies, n. It is thus seen that a vacancy undersaturation ($C_0/C > 1$) and the presence of a tensile stress ($P > 0$) should favour the growth of extrinsic faults.

As far as the kinetics of growth are concerned, a simple argument may explain some experimental results regarding the dependence of the SF length on temperature and oxidation time. The SF length is the distance between the two intersections of the Frank loop with the crystal surface and is affected only by the rate of growth in the direction of the intersection of the extra {111} planes with the surface. Since the growth of an extrinsic SF bounded by a Frank sessile loop takes place by a vacancy emission mechanism, the increase, Δl, of the SF length in a time Δt is proportional to the mean path $(D\Delta t)^{1/2}$ which is covered by a silicon atom (or by a vacancy) in a self-diffusion process. The self-diffusion coefficient, D, rather than the diffusion coefficient for vacancies, is expected to control the SF length, owing to the vacancy undersaturation near the silicon-oxide interface. We have, then, a simple relationship between the SF length, l, the self-diffusion coefficient, D, and the time, t, i.e.

$$l \approx (Dt)^{1/2} .$$

The expected dependence of l on $t^{1/2}$ was well satisfied for dry oxidation (see Fig. 5) whereas a steeper curve was obtained in a steam atmosphere: the reasons for this discrepancy are not understood. Moreover, twice the activation energy (i.e. 5.2 eV) which was found from plots of the SF length against reciprocal oxidation temperature, agrees with the activation energy for self diffusion in silicon as measured by means of radioactive tracers, namely 4.8 to 5.1 eV [24-27].

Although the proposed model seems to be satisfactory, at least at a qualitative level, an accurate picture of nucleation and growth processes of oxidation SF is difficult. Some of the reasons for this are: (i) the stress state at nucleation sites is unknown; (ii) the vacancy undersaturation, which is supposed to be the driving force for the growth process is also unknown. Further, it is also likely to depend strongly on the distance from the silicon-oxide interface, being greater at the interface itself; this may explain the

observed depth-to-length ratio of SFs which shows an enhanced growth rate near the surface; (iii) the interaction between the surface and the Frank dislocation line surrounding the fault should be taken into consideration.

5. Conclusion

Oxidation stacking faults in epitaxial silicon layers nucleate at crystallographic defects which appear as hillocks after a preferential etch. The emerging SFs lie in {111} planes. X-ray topography confirms their extrinsic nature and that the loop dislocation which limits the SF is of the Frank type. The SF length was determined for some oxidation temperatures, ambients and substrate orientations. In runs of the same duration, the length is controlled by an activation energy of 2.6 eV, regardless of the used oxidation atmospheres or substrate orientations. In isothermal runs, the SF length is a parabolic function of time when a dry oxidation is employed, while in steam oxidation the fault develops at a faster rate.

A model for growth of SFs is proposed, based on the undersaturation of vacancies near the silicon-oxide interface and the existence of tensile stress in the neighbourhood of the hillocks. In such conditions, vacancies diffuse away from the defect and a growth of the stacked layer results. Such a mechanism may be expected to depend upon the self-diffusion of silicon which is controlled by an activation energy in the region of 5 eV, sustantially confirming the experimental result.

Acknowledgement

The authors are grateful to Mr M. Scaffardi for processing the X-ray micrographs.

References

1. S. PRUSSIN, *J. Appl. Phys.* **43** (1972) 733.
2. K. V. RAVI, *J. Electrochem. Soc.* **120** (1973) 533.
3. I. R. SANDERS and P. S. DOBSON, *Phil. Mag.* **20** (1969) 881.
4. C. M. DRUM and W. VAN GELDER, *J. Appl. Phys.* **43** (1972) 4465.
5. F. J. WILHEIM and M. L. JOSHI, *ibid* **36** (1965) 2592.
6. K. V. RAVI and C. J. VARKER, *ibid* **45** (1974) 233.
7. A. W. FISHER and J. A. AMICK, *J. Electrochem. Soc.* **113** (1966) 1056.
8. J. E. LAWRENCE, *J. Appl. Phys.* **40** (1969) 360.
9. A. MAYER, *RCA Review* **31** (1970) 414.
10. Y. SUGITA and F. KATO, *J. Appl. Phys.* **42** (1971) 5847.
11. H. J. QUEISSER and P. G. G. VAN LOON, *ibid* **35** (1963) 3066.
12. E. BARSON, M. S. HESS and M. M. ROY, *J. Electrochem. Soc.* **116** (1969) 304.
13. H. J. QUEISSER and A. GOETZBERGER, *Phil. Mag.* **8** (1963) 1063.
14. M. CONTI and G. CORDA, *IEEE J. Sol. Stat. Circuits* **SC9** (1974) 124.
15. F. SECCO D'ARAGONA, *J. Electrochem. Soc.* **119** (1972) 948.
16. G. H. SCHWUTTKE and J. K. HOWARD, *J. Appl. Phys.* **39** (1968) 1581.
17. P. PENNING and D. POLDER, *Philips Res. Rep.* **16** (1961) 419.
18. P. PENNING, *ibid (suppl.)* **5** (1966) 1.
19. K. KOHRA and M. YOSHIMATSU, *J. Phys. Soc. Japan* **17** (1962) 1041.
20. J. MATSUI and T. KAWAMURA, *Jap. J. Appl. Phys.* **11** (1972) 197.
21. G. H. SCHWUTTKE, K. BRACK and E. W. HEARN, *Microelectronics and Reliab.* **10** (1971) 467.
22. G. R. BOOKER and W. J. TUNSTALL, *Phil. Mag.* **13** (1966) 71.
23. S. PRUSSIN, *J. Appl. Phys.* **43** (1972) 2850.
24. R. F. PEART, *Phys. Stat. Sol.* **15** (1966) KII9.
25. R. N. GHOSTAGORE, *Phys. Rev. Letters* **16** (1966) 890.
26. B. J. MASTERS and J. M. FAIRFIELD, *Appl. Phys. Letters* **8** (1966) 280.
27. J. M. FAIRFIELD and B. J. MASTERS, *J. Appl. Phys.* **38** (1967) 3148.

Received 5 November and accepted 20 November 1974.